

This is a repository copy of Dissolved nutrient gas uptake and fluid mixing by bubble-mediated mass transfer in tall fermenters — a theoretical study.

White Rose Research Online URL for this paper: https://eprints.whiterose.ac.uk/id/eprint/232799/

Version: Published Version

Article:

Chaffin, S., Monk, N.A.M. orcid.org/0000-0002-5465-4857, Rees, J.M. orcid.org/0000-0002-6266-5708 et al. (1 more author) (2024) Dissolved nutrient gas uptake and fluid mixing by bubble-mediated mass transfer in tall fermenters — a theoretical study. Food and Bioproducts Processing, 145. pp. 136-147. ISSN: 0960-3085

https://doi.org/10.1016/j.fbp.2024.03.004

Reuse

This article is distributed under the terms of the Creative Commons Attribution (CC BY) licence. This licence allows you to distribute, remix, tweak, and build upon the work, even commercially, as long as you credit the authors for the original work. More information and the full terms of the licence here: https://creativecommons.org/licenses/

Takedown

If you consider content in White Rose Research Online to be in breach of UK law, please notify us by emailing eprints@whiterose.ac.uk including the URL of the record and the reason for the withdrawal request.



ELSEVIER

Contents lists available at ScienceDirect

Food and Bioproducts Processing

journal homepage: www.elsevier.com/locate/fbp





Dissolved nutrient gas uptake and fluid mixing by bubble-mediated mass transfer in tall fermenters — A theoretical study

S. Chaffin a,b, N.A.M. Monk b,c, J.M. Rees b, W.B. Zimmerman d,*

- ^a Department of Physics and Mathematics, University of Hull, Hull HU6 7RX, UK
- ^b School of Mathematics and Statistics, University of Sheffield, Sheffield S3 7RH, UK
- ^c African Institute for Mathematical Sciences, P.O. Box LG DTD 20046 Legon, Accra, Ghana
- ^d Department of Chemical and Biological Engineering, University of Sheffield, Sheffield S1 3JD, UK

ARTICLE INFO

Keywords: Airlift bioreactors Microbubbles Process intensification Fungi Microprotein Fusarium venenatum

ABSTRACT

A laminar flow perturbation theory for small gas volume fraction in high aspect ratio bubble columns is developed. The model captures the approximate hydrodynamics, mass transfer, microbicidal gas consumption as well as the hydrostatic head appropriate to vessels in the range of 10–50 m heights. The model is validated against a finite element multiphysics two fluid bubbly flow model for limiting cases of low heights. The key parameter in the mixing is found to be the ratio between stripping length scale, and the hydro-static pressure variation. If this is small, the mixing efficiency in the unaerated region increases like the bubble radius to the -3rd power, but for large values it is independent of the bubble radius. The overall mass transfer continues to increase as the bubble radius decreases. We find that decreasing the bubble radius from 1 cm scale to 1 mm results in an order of magnitude increase in our mixing metric.

1. Introduction

The production of high protein content biomass (mycoprotein) by aerobic fermentation of Fusarium venenatum is an important contributor to enhancing sustainability of food production. The history and future relevance of the production of mycoproteins by the aerobic Ouorn process in fermentation vessels is reviewed by Wiebe (2002) and Finnigan et al. (2017, 2019). The first plant was conceived in the 1960s, built in the late 1970s, and began production in the early 1980s. The airlift loop design used is among the tallest fermenters, with three 50 m tall bioreactors with a volume of approximately 225 m³. The configuration creates coarse bubbles (1 cm diameter), some of which are coalescent into a central plume. A simple mass transfer calculation, for instance (Desai and Zimmerman, 2023a), demonstrates that at the top of a 50 m vessel in the main bubble column, only about 1% of the thermodynamically transferable oxygen will have dissolved in the aqueous media, due to the low interfacial area, which is consistent with the stripping calculations by Rees-Zimmerman and Chaffin (2021). This low degree of mixing, as well as low mass transfer rates, results in a culture which is oxygen starved in general. Hanotu et al. (2016) showed that in batch yeast propagators, conventional bubble transfer results in dissolved oxygen crashing to zero. The much greater surface area of injected microbubble clouds were necessary to achieve pseudo-steady dissolved oxygen levels at an adjustable level below saturation.

This illustrates a general principle: a key challenge in obtaining optimal growing conditions for biomass in both aerobic and anaerobic processes is obtaining sufficient mixing. Poor mixing can result in poor distributions of nutrients (Anderson et al., 1982) as well as poor control over the operating conditions (Jackson, 1985). Furthermore, current aeration methods in bioprocessing are costly. For instance, 15% of the total yeast production cost is attributed to aeration (Becze and Liebmann, 1944; Gélinas, 2016). The two most common conventional methods of mixing are to either drive the flow via mechanical stirring or to use a bubble column. While it is received wisdom that mechanical stirrers produce better mixing, the high shearing forces that result from the stirring can damage cells (Chisti and Moo-Young, 1986; Garcia-Ochoa et al., 2013). Conventional (unmixed) columns create a low stress environment, yet suffer from poor mass transfer rates. Rehman et al. (2015) show laboratory experiments with 55% increase in mass transfer rates via fluidic oscillation over steady flow in the same aeration system with the same pressure drop. Microbubble sparging has proved to be an attractive alternative to conventional mixers due to the high surface area to volume ratios achieved and low shear forces (Al-Mashhadani et al., 2015), although there is some debate about whether

E-mail address: w.zimmerman@sheffield.ac.uk (W.B. Zimmerman).

^{*} Corresponding author.

bubble breakup may damage cells (Gilmour and Zimmerman, 2020; Nienow, 2006).

Microbubbles produced by fluidic oscillation have been injected into a wide range of bioprocessing units for dosing nutrients or stripping product gases or volatile liquids, achieving high bubble fluxes. For instance, Desai et al. (2018) achieved an average bubble size of 7 μm with a bubble flux of around 1 hectare per square meter of diffuser per second, generated by tuning the air throughput and oscillation frequency through a sintered alumina diffuser with 2 μm sized pores. The same diffuser produced average bubble sizes of 400–500 μm with steady flow. Hence, evaluating the greater effectiveness of bubble sizes less than the coarse bubbles currently used in the tallest bioreactors is an important contribution to efforts to optimize growing conditions.

Hanotu et al. (2016) propagated a yeast strain (Saccharomyces cerevisiae) in a 3 L cylindrical Airlift Loop Bioreactor (ALB) made of perspex measuring 0.3 m and 0.14 m in height and base respectively. They achieved any desired dissolved oxygen level, controllable up to saturation, with this scalable configuration similar to bubble columns and the external airlift loop used for the Quorn process. Kaster et al. (1990) showed that microbubbles produced higher growth rates of Saccharomyces cerevisiae than conventional bubbles due to the increased oxygen transfer. Moreover, they found that increasing the mechanical stirring had no effect on the oxygen transfer, demonstrating that hydrodynamics from microbubbles leads to a well mixed system.

Scaling to commercial-scale vessels is typically impractical, so simulation of flow and gas exchange characteristics provides an important complementary approach. Laboratory scale geometric variations of this approach (volumes of 100-1000 L), were simulated numerically by Al-Mashhadani et al. (2015). This study demonstrated that the reduction of bubble size that occurs with microbubbles leads to a more uniform distribution of gas phase fraction and thus better mixing in the riser region. However the study did not allow mass transfer into the liquid phase or any up-take of the dosed gas. Extending the simulations to tall bioreactors, including mass transfer effects, requires substantial computation intensity, as well as appropriate modelling of hydrostatic pressure effects. Large aspect ratios always present a challenge to computational modelling of transport equations, but particularly in poorly mixed fermentation systems which have non-homogeneous, spatially distributed differences in cell or microbial culture density and concentration of secreted metabolites and substrate. Tall bioreactors, such as the 10-50 m high vessels used for F. venenatum, present a challenge to fermentation process design because hydrostatic pressure decreases with height over an appreciable range, typically 0.1–0.5 bar, respectively, for aqueous media. This influences mass transfer to gas phases, such as bubbles.

There is a massive diversity of potential bioproducts that can be found in fungal species, a large class of which could be produced in similar bubble aerated fermenters (Chambergo and Valencia, 2016) should suitable recovery and purification approaches be developed (Lonchamp et al., 2019). Of course, the composition of the centrate depends crucially on the composition of the media, and specifically the sugary feedstock used as the substrate. Hosseini et al. (2009) explored the design of the growth media as a modified Vogel medium using date sugar as the carbon source, optimizing over seven variables for the crude protein production. A similarly aimed study with different components found that the composition of date extract, Jaggery water and KH₂PO₄, were the most significant factors influencing protein and biomass production (Pandurangan et al., 2015). Date waste is the major novelty in the media composition optimization study of Reihani and Khosravi-Darani (2019). Bread waste has also been shown as potential feedstock to provide the sugary carbon source (Svensson et al., 2021).

Given the range of liquid media compositions and bioproducts that could be present in a tall bioreactor, a platform transport model should include, at a minimum, mass transfer between the bubble phase and the medium, and allow for the analysis of the effects of bubble size. Additionally, dissolved nutrient gas uptake, which gives an indication

of mixing efficiency and overall gas uptake, adaptable to *F. venenatum*, would be useful to inform scoping and design studies. Such a model should be extendable to metabolic modelling and cell growth kinetic studies, customized to the microbe being cultured. The nearest existing model in the literature is a 1-D (vertical) computational model applied to offgas composition inferences for mass transfer coefficients and ethanol stripping in a tall bioreactor, for a variant of *Geobacillus thermoglucosidasius* (Rees-Zimmerman and Chaffin, 2021). That model does not, however, treat hydrodynamics in sufficient detail to capture radial mixing.

In this paper, we develop a mathematical model to better understand the interplay of mass transfer, microbial uptake rate and bubble size in column bioreactors. Specifically, we will consider the laminar mixing from monodispersed bubbles in a viscous fluid. We restrict ourselves to laminar behaviour since, for highly viscous fluids, achieving turbulence with sensible shear rates can prove difficult (Sossa-Echeverria and Taghipour, 2015; de Jesus et al., 2017), particularly given that the medium is highly dissipative. Fig. 1 gives a process diagram of the layout of tall bioreactor with injected, monodisperse bubbles due to fluidic oscillation, which is representative of the class of bioreactors modelled in this paper. It should be noted that for food and bioproducts processing, good manufacturing practice requires that the diffuser be sterilizable. Commonly, that would be of stainless steel construction for steam cleaning and disinfection. Metal porous spargers, such as produced by Mott Corporation (Kazakis et al., 2008) or plate or sieve spargers for which (Kulkarni and Joshi, 2011) have developed a design selection approach, are likely to be suitable.

Fermentation media with hyphae as free mycelia at high biomass concentrations results in high viscosity, leading to issues with gasliquid mass transfer, liquid mixing and a generally complex rheology (Porcel et al., 2005). Bubbles introduced into laminar flow in a highly viscous media could maintain laminar flow if they rise in concert. Crabtree and Bridgwater (1969) provide a mechanistic argument for the non-coalescence of chains of bubbles being hydrodynamically stabilized in laminar flow as they rise. Their studies and subsequent studies of chain bubbling point to vertical stabilization when the spacing between rising bubbles is not less than 2 bubble diameters for monodisperse bubbles. The creation of monodisperse bubbles and maintenance of laminar flow has been shown with bubbles generated by fluidic oscillation by jet diversion (Zimmerman et al., 2011). Although renowned for microbubble generation, the mechanism has recently been shown to produce nearly uniformly sized and spaced fine bubbles in highly viscous ionic liquids, tuneable to be smaller than steady flow with random bubble release and coalescence from the same porous diffuser, for instance (Desai and Zimmerman, 2023b). Furthermore, it is well known that surfactants (Ribeiro and Lage, 2004) or ionic salts (Ribeiro and Lage, 2005) in sufficient concentrations oppose bubble coalescence, due to the double layer induced repulsion effect, akin to colloidal stabilization. Hyphae fermentation broth is likely to be surfactant and nutrient salt laden, so opposing bubble coalescence and associated with an additional repulsive force to stabilize nearly monodispersed and uniformly spaced bubbles.

An important feature of our new baseline bubble mediated transport model for tall fermenters is our construction of an approximate mathematical model for the desired independent variables in analytic, closed form. The advantage of a closed-form model that captures these effects is that the computational intensity to include additional biochemical and biomass kinetic components that are spatially distributed and even transient for batch or semi-batch operations, is negated.

The paper is organized as follows. In Section 2, we present a suitable set of governing equations. These are analogues of those used for stripping ethanol mediated via bubbles (Rees-Zimmerman and Chaffin, 2021). Subsequently, we analyse these by perturbation methods to find an analytic approximation in the case of hydrostatic pressure-dominated laminar flows of the liquid and bubble phases. In Section 3, the predictions from the perturbation theory model are compared

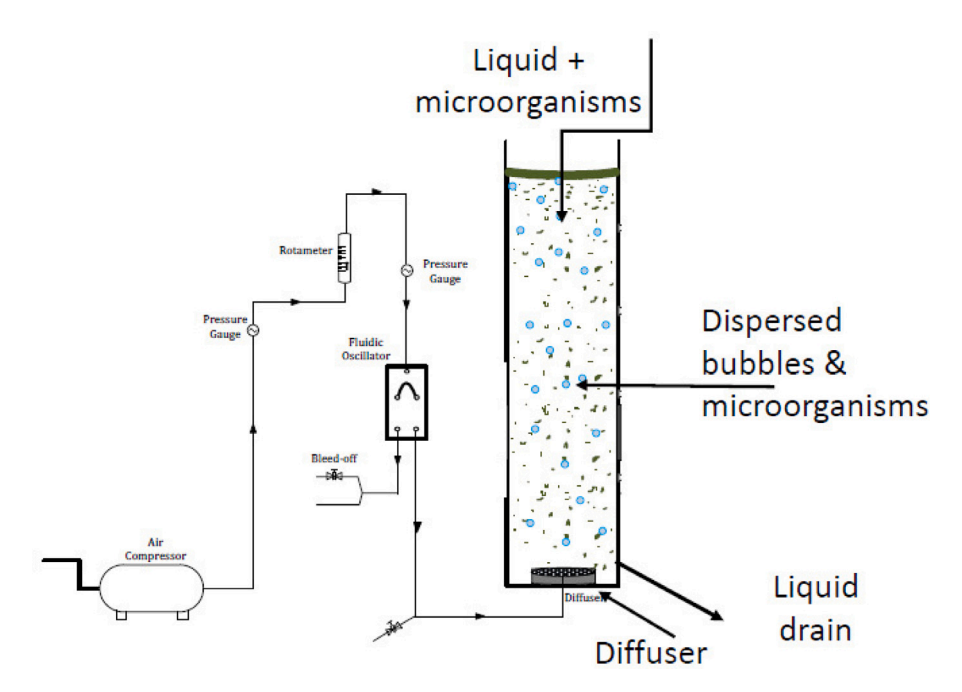


Fig. 1. A schematic diagram of a tall bubble bioreactor with key features of air (oxygen) source, fluidic oscillator for monodisperse bubble formation, and bioreactor with diffuser flush with the floor.

with fully resolved finite element method computations of the 2-D axisymmetric bubbly flow model, validating the range of bubble sizes and diffuser profile on the base of the fermenter which are well approximated. In Section 4, the hydrodynamics model is augmented with mass transfer and microbial uptake to meet nutrient gas demand from dissolved gas in the media. The results are explored and discussed. In Section 5, the conclusions are drawn, particularly highlighting the importance of bubble size on system performance.

2. Governing equations

We will consider a cylindrical geometry of radius L and height H containing a fluid with density ρ_l and viscosity μ . Thus, we will perform our analysis with polar coordinates $r=\sqrt{x^2+y^2}$ and z with 0 < r < L, 0 < z < H which are shown in Fig. 2. Bubbles will be introduced to the system by a diffuser which is flush with the base of the cylinder located at z=0. The diffuser is circular with a radius r_d through which the gas phase enters the system with a volume flux Q. There are solid walls located on z=0, r=L and a free surface open to the atmosphere at z=H. A sketch of the system is shown in Fig. 2.

For small gas phase fractions $\phi_{\rm g}$, momentum conservation in the liquid phase is given by

$$\phi_{l}\rho_{l}\left(\mathbf{u}_{l}\cdot\nabla\right)\mathbf{u}_{l} = -\nabla p + \mu\nabla\cdot\left(\phi_{l}\dot{\mathbf{y}}\right) + \phi_{l}\rho_{l}\mathbf{g}.\tag{1}$$

Here u_l is the liquid velocity field, $\dot{\gamma} = \nabla u_l + \nabla u_l^T$ is the rate of strain tensor. The rate of strain tensor is symmetric by design, having been formed by the velocity gradient tensor and its transpose. Panton (1984) ϕ_l is the liquid phase fraction, which couples to the gas phase fraction by $\phi_l = 1 - \phi_g$. Mass conservation in the liquid and gas phase are respectively given by

$$\nabla \cdot \boldsymbol{u}_l = 0, \tag{2}$$

$$\nabla \cdot \left(\rho_g \mathbf{u}_g \phi_g \right) = 0. \tag{3}$$

The pressure p and gas density ρ_g are linked via the ideal gas law

$$\rho_{\rm g} = \frac{p}{RT}.\tag{4}$$

We close the system by assuming an isothermal approximation, i.e. the temperature T is constant. However, we have not included the

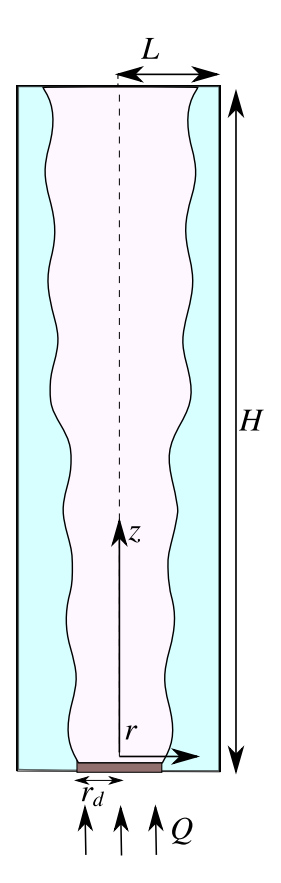


Fig. 2. Sketch of the diffuser setup

momentum equation for the gas phase, and thus we have insufficient equations to find the gas velocity u_g . To simplify the system we will use the algebraic slip formulation (Mikko et al., 1996; Swiderski et al., 2016; Sokolichin et al., 2004). The slip velocity, which is the difference between the local velocity of the bubble and that of the liquid phase,

is given by $u_{slip} = u_g - u_l$, couples to the pressure by

$$\nabla p = -\frac{3\rho_l C_d}{4d_b} \left| \mathbf{u}_{slip} \right| \mathbf{u}_{slip}. \tag{5}$$

The drag constant C_d is chosen to be consistent with the Hadamard Rybczynski velocity (Abdulrazzaq et al., 2016), which is given by $C_d = \frac{8\mu_l}{a\rho_l|\mathbf{u}_{slip}|}$. We can rearrange Eq. (5) to give

$$\mathbf{u}_{g} = \mathbf{u}_{l} - \frac{a^{2}}{3\mu_{l}} \nabla p. \tag{6}$$

Eqs. (1)–(6) form the closed system of equations that we will solve in the following sections. It should be noted that in Eq. (5), we have implicitly assumed that the bubbles are mono-dispersed, with a constant bubble radius a.

2.1. Boundary conditions

As no liquid leakage occurs at any of the walls or the free surface it follows that

$$\mathbf{u} \cdot \mathbf{n} = 0 \tag{7}$$

on all the boundaries. For the walls, excluding the surface z=H, we will assume a no-slip condition

$$u_l = 0. (8)$$

As a result of the no leakage condition above the diffuser, the normal component of the gas velocity is given purely by the Hadamard formula $U_{hr}=\frac{1}{3}\mu^{-1}a^2g\rho_l$. From mass conservation, it follows that for a uniform inlet $Q=\pi r_d^2 U_{hr} \phi_g$. Hence, the boundary condition on gas phase fraction above the diffuser is given by

$$\phi_g \bigg|_{z=0} = \Gamma = \frac{Q}{\pi r_d^2 U_{hr}}.$$
(9)

2.2. Perturbation solution

The parameter Γ , although indicative of the gas phase fraction at the inlet is also the ratio of the liquid velocity field scale $U_l = \frac{Q}{\pi r_s^2}$ to the buoyant velocity scale U_{hr} . Throughout the rest of this article will assume that Γ is small. Employing the scalings $p = \rho_l g L \hat{p}, u_l = U_l \hat{u}, r = L \hat{r}, z = L \hat{z}, \nabla = L^{-1} \hat{\nabla}$, we derive the non-dimensional form of the system (1)–(3)

$$\alpha^2 Re \Gamma \phi_l \left(\hat{\mathbf{u}} \cdot \hat{\nabla} \right) \hat{\mathbf{u}} = -\hat{\nabla} \hat{\mathbf{p}} + \alpha^2 \Gamma \hat{\nabla} \cdot \left(\phi_l \hat{\mathbf{y}} \right) + \phi_l, \tag{10}$$

$$\hat{\nabla} \cdot \hat{\boldsymbol{u}} = 0, \tag{11}$$

$$\hat{\nabla} \cdot \left(\hat{p} \left(\phi_{\sigma} \left(\hat{\nabla} \hat{p} - \Gamma \hat{u} \right) \right) \right) = 0. \tag{12}$$

The parameter $\alpha=\frac{a}{\sqrt{3}L}$ is the ratio of the bubble diameter to the length scale of the system which is \ll 1. The parameter Re is the Reynolds number for a Newtonian fluid given by $\frac{U_l\rho_lL}{\mu_l}$ which will assume to be $\mathcal{O}(1)$. It is convenient to drop the $\hat{}$ notation, henceforth p,z,u,r,∇ will denote dimensionless quantities unless stated otherwise.

When $\Gamma=0$, we have no gas flux into the system and thus $\phi_l=1$, and the solution to (10)–(12) reduces to a hydro-static state. We seek a solution around this hydrostatic limit by considering a regular perturbation expansion in the form

$$p = \hat{p}_0 - z + \Gamma p^{(1)} + \mathcal{O}(\Gamma^2), \tag{13}$$

$$\mathbf{u}_{l} = \mathbf{u}^{(1)} + \mathcal{O}(\Gamma),\tag{14}$$

$$\phi_1 = 1 - \Gamma \phi^{(1)} - \Gamma^2 \phi^{(2)} + \mathcal{O}(\Gamma^3), \tag{15}$$

where $\hat{p}_0 = \frac{p_0 + \rho_I g H}{\rho_I g L}$. For ease of notation it is helpful to decompose the bubble velocity field into its radial and vertical component via

 $\mathbf{u}^{(1)} = u_1 \mathbf{e}_r + w_1 \mathbf{e}_z$. We express the boundary conditions in terms of the perturbed quantities as

$$u_1 = w_1 = 0$$
 on $r = 1$, (16)

$$u_1 = 0, \ w_1 \text{ is finite} \quad \text{on } r = 0 \ ,$$
 (17)

$$w_1 = 0, p^{(1)} = 0 \quad \text{on } z = \frac{H}{I} ,$$
 (18)

$$w_1 = 0, \phi^{(1)} = F(r), \ \phi^{(2)} = 0 \quad \text{on } z = 0.$$
 (19)

The function F(r) takes into account the fact that the diffuser does not cover the entire base and is defined as

$$F(r) = \begin{cases} 1 & \text{for } r \le I \\ 0 & \text{for } r > I, \end{cases}$$
 (20)

where $I = \frac{r_d}{L}$. The leading order mass conservation in the gas phase results in

$$\frac{\partial}{\partial z} \left(\left(\hat{p}_0 - z \right) \phi^{(1)} \right) = 0. \tag{21}$$

This gives the phase fraction to leading order term as

$$\phi^{(1)} = F(r) \left(1 - \frac{z}{\hat{p}_0} \right)^{-1}. \tag{22}$$

The leading order phase fraction term is concentrated in the region above the diffuser. Coalescence is known to occur mostly in the reverse flow wall region (Rahman et al., 2002). Hence we can expect the effects of bubble coalescence to be minor, thus justifying our assumption that the system will be well modelled by monodispersed bubbles. The $\mathcal{O}(1)$ order term in the momentum equation reduces to the hydro-static case, however at $\mathcal{O}(\Gamma)$ we find

$$-\nabla p + \alpha^2 \nabla^2 \boldsymbol{u}^{(1)} + F(r) \left(1 - \frac{z}{\hat{p}_0} \right)^{-1} = \alpha^2 Re \left(\boldsymbol{u}^{(1)} \cdot \nabla \right) \boldsymbol{u}^{(1)}, \tag{23}$$

where $u^{(1)}$ satisfies the solenoidal constraint $\nabla \cdot u^{(1)} = 0$ due to Eq. (11). Eq. (23) is equivalent to the Navier stokes equation with an inhomogeneous forcing term which arises from buoyancy forces from variations in the phase fractions. Though in the limit of $Re \to 0$ it is possible to solve analytically in a rectangular domain using an infinite sum of Papkovich–Fadle eigenfunctions (Joseph, 1977; Gaskell et al., 1998), we will deploy another approximation. Let us assume that the tank height H is much larger than its horizontal width L, i.e. $\frac{L}{H} = \varepsilon \ll 1$. Where it follows that r is $\mathcal{O}(1)$ and z is $\mathcal{O}(\varepsilon^{-1})$. From mass conservation and the requirement that the buoyancy term must to be retained to drive the flow, the variables must scale as: $u_1 \sim \mathcal{O}(\varepsilon)$, $w_1 \sim \mathcal{O}(1)$ and $p_1 \sim \mathcal{O}(\varepsilon^{-1})$. Hence, the leading terms for (1) are

$$\frac{\partial p_1}{\partial r} = 0, (24)$$

$$-\frac{\partial p_1}{\partial z} + \alpha^2 \frac{1}{r} \frac{\partial \left(r \frac{\partial w_1}{\partial r}\right)}{\partial r} + F(r) \left(1 - \frac{z}{\hat{p}_0}\right)^{-1} = 0, \tag{25}$$

where we assume $Re \cdot \varepsilon$ is small. Note that as we have lost the $\frac{\partial^2 w_1}{\partial z^2}$ term, we cannot implement the velocity component on the boundary conditions (18) and (19). As such there will be regions near the z=0, z=H where the effect of this term will be important; however for the bulk flow our approximation should capture the dominant physics.

We can solve (24) and (25) to give

$$w_{1} = \frac{1}{\alpha^{2}} \left[\frac{r^{2}}{4} \frac{\partial p_{1}}{\partial z} + A(z) \ln r + B(z) - G(r) \left(1 - \frac{z}{\hat{p}_{0}} \right)^{-1} \right], \tag{26}$$

where $G(r) = \int_0^r \frac{1}{r'} \left(\int_0^{r'} r'' F(r'') dr'' \right) dr'$. The function G can be written more succinctly as

$$G(r) = \begin{cases} \frac{r^2}{4} & \text{for } r \le I, \\ \frac{l^2}{4} & \left(1 + 2\ln\left(\frac{r}{I}\right)\right) & \text{for } r > I. \end{cases}$$
 (27)

The constants A, B can be found by requiring $w_1(0)$ to be non-singular and $w_1(1) = 0$. This results in

$$w_1 = \frac{1}{\alpha^2} \left[\frac{(r^2 - 1)}{4} \frac{\partial p_1}{\partial z} - (G(r) - G(1)) \left(1 - \frac{z}{\hat{p}_0} \right)^{-1} \right]. \tag{28}$$

As there is no net mass flux through each z plane, it follows that

$$\int_{0}^{1} r w_{1} \, \mathrm{d}r = 0. \tag{29}$$

Using (28) with (29) gives the pressure gradient

$$\frac{\partial p_1}{\partial z} = 2I^2 \left(1 - \frac{z}{\hat{p}_0} \right)^{-1} \left(1 - \frac{I^2}{2} \right). \tag{30}$$

Eqs. (28) and (30) give the vertical component of the velocity field. We can integrate using boundary condition (18) to give the absolute pressure correction as

$$p_1 = -2\hat{p}_0 I^2 \left(1 - \frac{I^2}{2} \right) \ln \left(\frac{1 - \frac{z}{\hat{p}_0}}{1 - \frac{\varepsilon^{-1}}{\hat{p}_0}} \right). \tag{31}$$

To get the radial component of the velocity field we can use massconservation to give

$$\frac{1}{r}\frac{\partial ru_1}{\partial r} = -\alpha^{-2} \left(\frac{\partial^2 p}{\partial z^2} \frac{r^2 - 1}{4} - \frac{1}{\hat{p}_0} \left(1 - \frac{z}{\hat{p}_0} \right)^{-2} (G(r) - G(1)) \right). \tag{32}$$

Using boundary conditions (7) and (8), the velocity field is given by

$$u_1 = -\hat{p}_0^{-1} \left(1 - \frac{z}{\hat{p}_0} \right)^{-2} U(r), \quad w_1 = \left(1 - \frac{z}{\hat{p}_0} \right)^{-1} W(r), \tag{33}$$

where

$$\begin{split} U(r) &= r^{-1}\alpha^{-2} \left[\frac{1}{8} I^2 \left(1 - \frac{I^2}{2} \right) r^2 \left(r^2 - 2 \right) - K(r) \right], \\ W(r) &= \alpha^{-2} \left[\frac{1}{2} \left(r^2 - 1 \right) I^2 \left(1 - \frac{I^2}{2} \right) - G(r) + G(1) \right], \end{split}$$

and the function K(r) is given by

$$K(r) = \int_{0}^{r} r \left(G(r') - G(1) \right) dr$$

$$= \begin{cases} \frac{1}{16} \left(r^{4} - 2r^{2}I^{2} \right) + \frac{1}{4}I^{2}r^{2}\ln(I) & \text{for } r < I \\ \frac{1}{4}I^{2}r^{2}\ln r + \frac{1}{16} \left(I^{4} - 2r^{2}I^{2} \right) & \text{for } r \ge I. \end{cases}$$
(34)

Eqs. (28) and (33) can be integrated to arrive at the Stokes stream function

$$\Psi = \alpha^{-2} \left(\frac{1}{16} r^2 \left(r^2 - 2 \right) \frac{\partial p}{\partial z} - \left(1 - \frac{z}{\hat{p}_0} \right)^{-1} K(r) \right). \tag{35}$$

Having derived the stream-function, we now have a complete description of the leading order dynamics of the liquid velocity field. This will be key in our later analysis of the effects of mixing in Section 4. However we will validate the accuracy of our asymptotically derived results by numerical simulation in Section 3.

3. Numerical results

We now compare our analytical results to a full numerical solution using the finite element method software COMSOL Multiphysics, where we solve the full system of Eqs. (1)–(6). We take our geometry to be a cylinder with radius 10 cm and height 1 m with the diffuser radius 2.5 cm with a flow rate of 100 mlmin⁻¹. We choose a viscosity value of 0.1[Pa s], which is a similar order of magnitude to reported viscosities values for YPD (yeast extract peptone dextrose) medium used to grow yeast (Calahorra et al., 2009). The boundary conditions are those from (7) to (9) with a natural outlet condition on $z = \frac{H}{I}$.

We plot the model prediction of the pressure correction and of the velocity field along the central axis r = 0 as functions of bubble radius a

in Figs. 3–5. We find that both the pressure correction and momentum transferred into the liquid are accurately predicted for bubble radius greater than 4 mm. For smaller bubble radii there is a significant overprediction in the velocity magnitude. The breakdown in the solution is not that Γ becomes large but that the liquid velocity is same order as the buoyant pressure driven velocity, i.e. in $(12) \nabla p$ is the same size as $\Gamma \hat{u}$. We can see this as liquid velocity $\Gamma \hat{u}$ from (35) that the velocity increases as a^{-4} whereas Γ only increases as a^{-2} .

4. Mass transfer

4.1. Governing equations

In the previous section we have shown that the analytic solution gives a good approximation of the momentum transferred from the gas into the liquid phase. The effect of momentum transfer for small bubbles has been proposed as a mechanism to increase liquid mixing in reactor vessels (Zimmerman et al., 2008). To quantify how well mixed the system is, we require mass transfer from the bubble into the liquid phase. In this section we will extend the model to include mass transfer from the bubble to the liquid, as well as a demand on the liquid phase concentration due to biomass growth. The mass transfer between the bubble and liquid phases will be modelled via Henry's law, which results in the inclusion of a mass source term to Eq. (3) (Rzehak and Krepper, 2016)

$$\nabla \cdot \left(\rho_g \mathbf{u}_g \phi_g \right) = -6K_I \phi_g a^{-1} \rho_I \left(H_e \frac{\rho_g}{\rho_I} - Y_I \right). \tag{36}$$

Here Y_l is the phase fraction of the dissolved gas in the liquid phase and H_e is the dimensionless Henry's constant. To close the system we must include a conservation for Y_l which is given by

$$\nabla \cdot \left(\mathbf{u}_l \phi_l \rho_l Y_l \right) = 6K_l \phi_g a^{-1} \rho_l \left(H_e \frac{\rho_g}{\rho_l} - Y_l \right) - rXY_l. \tag{37}$$

The last term accounts for the dissolved gas being taken up by the microorganisms that are being cultured, where the parameter rX is the gas uptake rate. In well-aerated conditions, a more appropriate relation for the uptake rate would be of the form

$$\frac{rXY_l}{1 + \frac{Y_l}{Y_0}},\tag{38}$$

where Y_0 is a positive constant. This form captures a saturating uptake rate when the system is well aerated. However, conditions in realistic bioreactors are such that dissolved gas is a limiting factor for microorganisms. Under these conditions, it is appropriate to use a linear uptake rate, which facilitates the mathematical analysis of the system.

Before we derive our solution, in addition to previous expansions (13)–(15) we require a perturbation expansion for Y_l as well. In the limit $\Gamma \to 0$, we expect $Y_l \to 0$, which motivates the scaling

$$Y_{l} = \Gamma Y + \mathcal{O}(\Gamma^{2}). \tag{39}$$

We will now derive the leading order asymptotic behaviour of Eqs. (2), (6), (36), and (37).

4.2. Flow field

If we non-dimensionalize as in Section 2.2, Eq. (2) becomes

$$\nabla \cdot (\hat{p}(-\nabla \hat{p} + \Gamma \hat{u})\phi) = -\mathcal{K}\phi\hat{p},\tag{40}$$

where $\mathcal{K} = 6H_eLK_la^{-1}U_{hr}^{-1}$. To leading order we have

$$\frac{\partial}{\partial z} \left(\left(\hat{p}_0 - z \right) \phi \right) = -\mathcal{K} \phi \left(\hat{p}_0 - z \right). \tag{41}$$

We can solve this for the gas phase fraction

$$\phi = F(r) \left(1 - \frac{z}{\hat{p}_0} \right)^{-1} e^{-\mathcal{R}z},\tag{42}$$

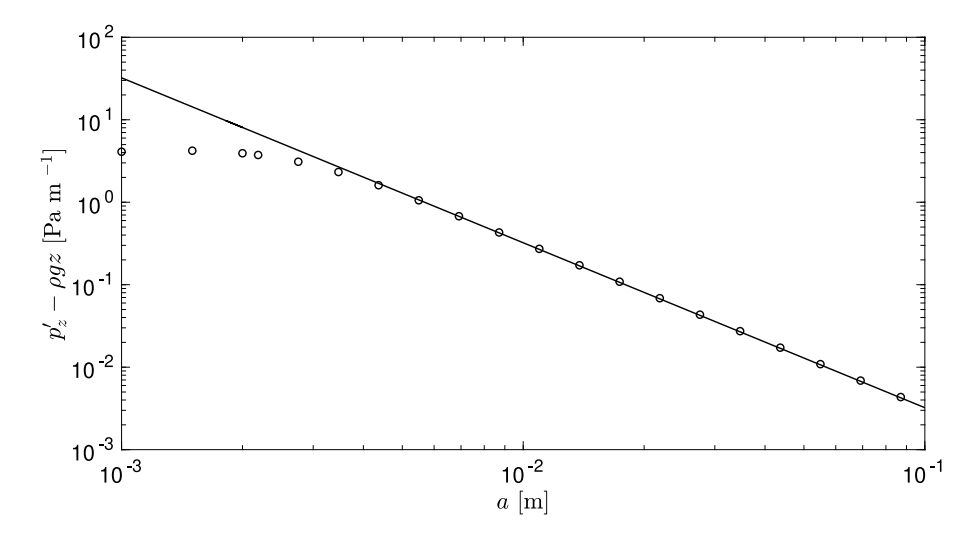


Fig. 3. The additional dimensional pressure gradient (after subtracting the hydro-static gradient) as a function of bubble radius a. The numerical and analytic solutions are denoted by circular marks and the solid line, respectively.

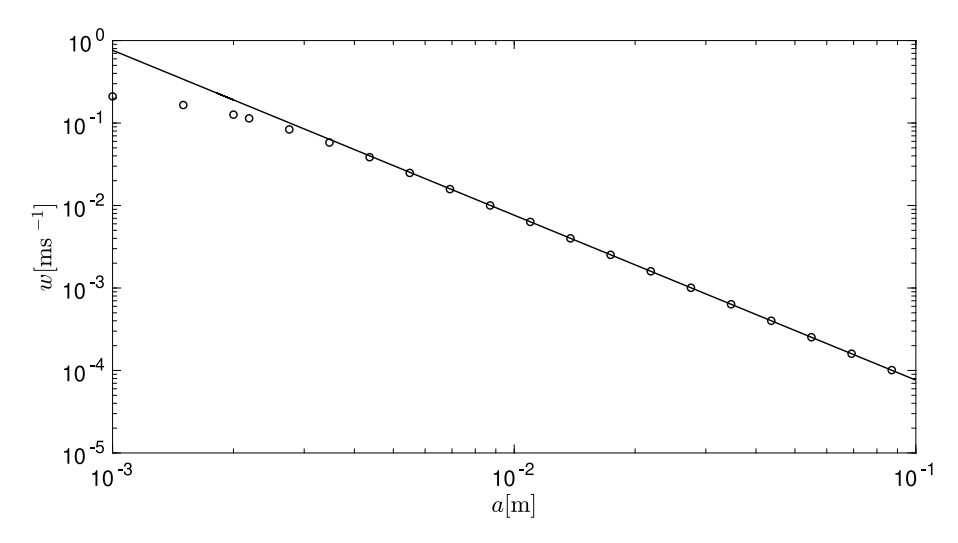


Fig. 4. The dimensional velocity w along the centre line (r=0) and on the plane $z=\frac{H}{2L}$ as a function of bubble radius a. The numerical and analytic solutions are denoted by circular marks and the solid line, respectively.

where F(r) is given by Eq. (20), which is similar to the leading order buoyancy phase fraction with a scaling factor due to stripping. To get the full dynamics of the system we will find the induced velocity field. Proceeding as in Section 2, we recover the expression for the velocity field:

$$u_1 = -\left(\hat{p}_0^{-1} \left(1 - \frac{z}{\hat{p}_0}\right)^{-2} - \mathcal{X}\left(1 - \frac{z}{\hat{p}_0}\right)^{-1}\right) e^{-\mathcal{X}z} U(r), \tag{43}$$

$$w_1 = W(r) \left(1 - \frac{z}{\hat{p}_0} \right)^{-1} e^{-\mathcal{X}z},$$
 (44)

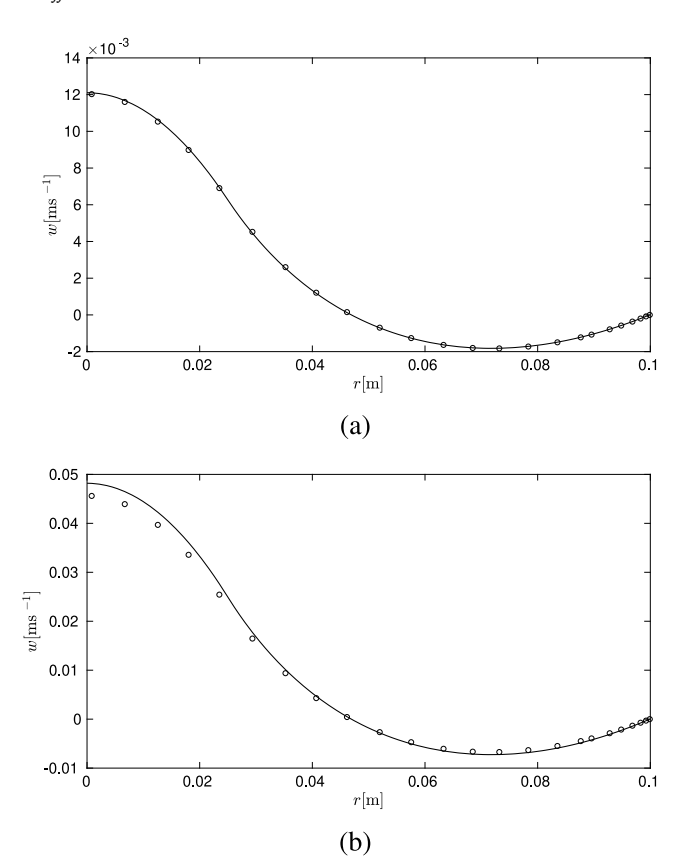
which reduce to the expressions in Eq. (33) in the limit $\mathcal{K} \to 0$. The re-circulating streamlines are shown in Fig. 6 for both the stripping and purely hydrostatic cases. The reversal of the radial component of velocity can be seen to occur in Eq. (43). If \mathcal{K} is larger than \hat{p}_0^{-1} , the liquid velocity field will be "pushed" out of the aerated region. When this is not the case, (as with the hydrostatic case) the liquid velocity will be "pulled" into the aerated region. We can interpret this physically as the inhomogeneity in the z-direction being fundamental to inducing the liquid velocity field; without it the flow would be unidirectional in the z-direction. However, the decrease of hydrostatic pressure with height results in a monotonically increasing phase fraction, whereas stripping results in a monotonically decreasing phase fraction. These two competing effects result in different streamline configurations.

In both cases there will be a thin strip at the top or bottom of the tank where this will not hold, which allow the streamlines to connect. We can capture this in our model because of the large aspect ratio assumption.

4.3. Liquid phase fraction

In the mass transfer problem there are two competing z scales, \hat{p}_0 from the pressure variation and \mathcal{K}^{-1} from mass transfer. We will focus on the two cases where mass-transfer happens more quickly (slowly) than the effects due the pressure variation. In these regimes we require the degassing scale to be smaller (larger) than the length scale that the pressure variations occur over i.e. $\omega = \mathcal{K}\hat{p}_0$ is large (small). Using the parameters from Fig. 6 and choosing an approximate $K_l = 5 \times 10^{-4} \text{ ms}^{-1}$, which is the measured K_l of oxygen bubbles in water (Lebrun et al., 2021), gives ω approximately in range 0.05 to 50 if the radius varies between 1 cm to 1 mm. So our assumption will hold in this regime. To get a broad spectrum of values we will solve the dynamics for ω large (very small bubbles) and for ω small (large bubbles).

We will apply the scalings from Section 2 along with $\hat{z} = \frac{z}{\hat{p}_0}$, and again drop the $^{\wedge}$ notation. The first metric we will use is the total



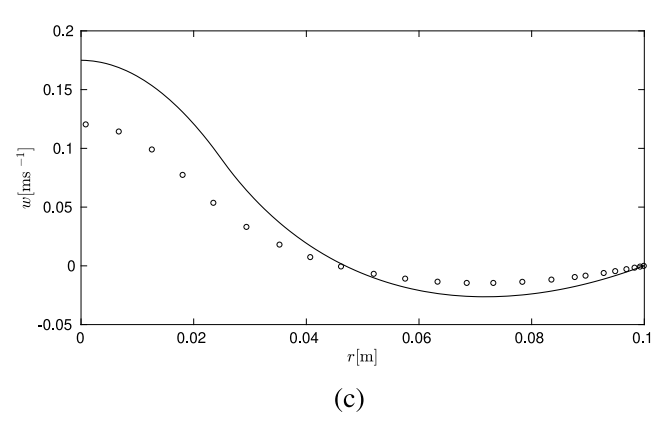


Fig. 5. The dimensional vertical velocity profile along the centre plane $z=\frac{H}{2L}$ for a=8 mm, 4 mm, 2 mm for graphs (a), (b) and (c). The numerical and analytic solutions are denoted by circular marks and the solid line, respectively.

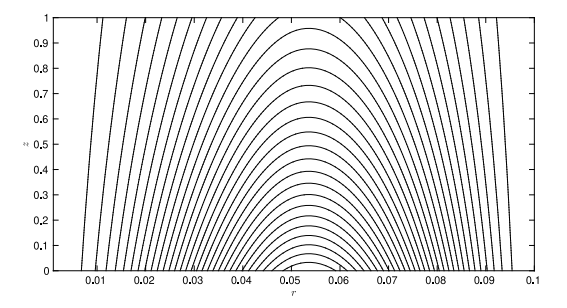
dimensionless flux from the gas phase into the liquid phase which, using (42), is defined by

$$M_{\text{eff}} = \Gamma \int_0^{\frac{H}{L}} \int_0^1 r\omega (1-z) \phi \, dr \, dz,$$

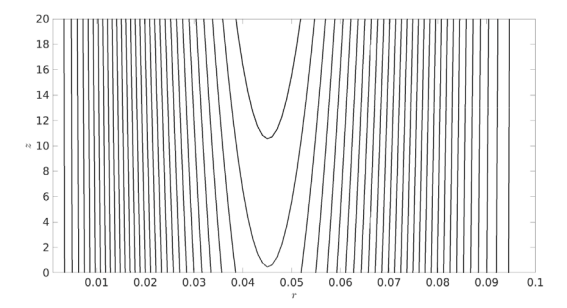
which has asymptotic behaviours $M_{\rm eff}\sim \frac{1}{2}\Gamma I^2\hat{p}_0$ as $\omega\to\infty$ and $M_{\rm eff}\sim \frac{1}{4}\Gamma I^2\omega\frac{H}{L}$ as $\omega\to0$. Hence, we see that the efficiency increases like a^{-2} in the small bubble regime and as a^{-5} for large bubbles. This is indicative of the total gas transfer, however it does not indicate how dispersed or well mixed the dissolved gas is. To quantify this we need to solve for the liquid phase fraction.

Eq. (37) becomes to leading order in Γ

$$(\hat{\boldsymbol{u}} \cdot \nabla) Y = \mathcal{L} F(r) e^{-\omega z} - r \widehat{X} Y, \tag{45}$$



(a) Sample dimensional stream-lines including mass transfer with parameters: a=2mm, L=10cm, H=20m, $\mathcal{K}=1$, $\mu_l=0.1$ Pa.s, $\rho_l=1000$ kgm⁻³.



(b) Dimensional stream-lines for the solely hydro-dynamics case with a=2mm, L=10cm, H=20m, $\mu_l=0.1\text{Pa.s}$, $\rho_l=1000\text{kgm}^{-3}$.

Fig. 6. Re-circulating streamlines for both the stripping (a) and purely hydrostatic (b)

where $\mathcal{L} = \frac{6K_IL^2gH_e}{aU_IRT}$, $\widehat{rX} = \frac{rXL}{\rho_IU_I}$. We will now solve this equation for large ω , which we will call the quick degassing case, and for small ω , which we will call the slow degassing case.

4.4. Quick degassing

We can see by the method of dominant balance that there is a solution of (45) such that

$$Y \sim \frac{\mathscr{L}F(r)}{r\widehat{\chi}}e^{-\omega z}$$
 as $\omega \to \infty$. (46)

Hence the scaled variable Y_l increases like a^{-3} in the aerated region, until the negative feedback term from Henry's law becomes important.

This solution can be noted by observing that both the dosing is balanced by the uptake, which are both $\mathcal{O}(e^{-\omega z})$. The advection terms are $\mathcal{O}(\omega e^{-2\omega z})$ which are much smaller. The balance between dosing and uptake is only possible when the bubbles are present to leading order, i.e. when $F(r) \neq 0$ or equivalently r < I. For the r > I region, taking the leading order terms, the governing equations are

$$p_0^{-1} \left(\omega (1-z)^{-1}\right) e^{-\omega z} U(r) \frac{\partial Y}{\partial r} + p_0^{-1} (1-z)^{-1} e^{-\omega z} W(r) \frac{\partial Y}{\partial z} = -\widehat{rX} Y. \tag{47}$$

As we are solving for large ω , we can use a multiple scales approach to separate the fast length scale $=\omega z$ from the slower length scale z. Along with the transformation r=s and $\tau=p_0^{-1}(1-z)^{-1}e^{-\omega z}rU(r)$, we can transform (47) into

$$\omega \tau \frac{\partial}{\partial s} Y = -s \widehat{rX} Y, \tag{48}$$

which has general solution

$$Y = A(z, \tau)e^{-\frac{1}{2}r\widehat{X}s^2\omega^{-1}\tau^{-1}}.$$
 (49)

Note that here A is a function of τ and z, (due to the multiple scales approach) and can be found by matching up with the solution (46) along r = I, which leads to

$$A = (1 - z) \frac{\mathcal{L}}{\widehat{rX}IU(I)} \hat{p}_0 \tau e^{\frac{1}{2}\widehat{rX}\omega^{-1}I^2\tau^{-1}}.$$
 (50)

Thus, after some algebra, we have the final solution for the dissolved gas concentration:

$$Y = \begin{cases} \frac{\mathcal{L}}{\widehat{rX}} e^{-\omega z} & r \le I \\ \frac{\mathcal{L}rU(r)}{\widehat{rX}IU(I)} e^{-\widehat{rX}\widehat{p}_0 B(r)(1-z)\omega^{-1}e^{\omega z}} e^{-\omega z}, & B(r) = \frac{1}{2} \frac{(r^2 - I^2)}{rU(r)} & r > I, \end{cases}$$
 (51)

where the liquid mass phase fraction Y_l can be recovered using Eq. (39).

4.5. Characterizing mixing (quick degassing case)

We have previously addressed the question of how efficiency depends on the bubble radius. We now address a further two key questions: how well mixed is the vessel and how efficient is the dosing?

To quantify the mixing, we first note that the region directly above the diffuser (r < I) will be well dosed due the large amounts of bubbles present. However, in the unaerated region (r > I) this is no longer the case. We will quantify the mixing by asking how well dosed is the remaining unaerated region of the vessel? The dosing in this region (to leading order) is via recirculating motions advecting the liquid phase fraction into the unaerated area, and this is what we wish to quantify.

As a metric for mixing we will use the total liquid phase in the unaerated region, i.e.

 $M_{\rm mi}$

$$= \Gamma \hat{p}_0 \int_0^{\frac{H}{L\hat{p}_0}} \int_I^1 \frac{\mathcal{L}rU(r)}{r\widehat{X}IU(I)} \exp\left\{-\omega z - r\widehat{X}\hat{p}_0 B(r)(1-z)e^{\omega z}\omega^{-1}\right\} r dr dz.$$
(52)

We can use Laplace's theorem to approximate this integral by

$$\Gamma \hat{p}_0 \omega^{-1} \int_I^1 \frac{\mathcal{L}r^2 U(r)}{\widehat{rX} IU(I)} e^{-\omega^{-1} \widehat{rX} \hat{p}_0 B(r)} dr.$$
 (53)

One cannot immediately perform a naive regular perturbation expansion of the integral in powers of ω^{-1} due to the singularity in B at r=1. By separating the integral into a small region around the singular point r=1, the contribution from the singularity can be shown to be $\mathcal{O}(\omega^{-\frac{3}{2}})$ and be neglected. Hence, the leading order term is given by

$$\begin{split} M_{\text{mix}} &\sim \Gamma \hat{p}_0 \omega^{-1} \frac{\mathcal{L}}{rXIU(I)} \int_I^1 r^2 U(r) \, \mathrm{d}r \\ &= \frac{\Gamma \mathcal{L} \omega^{-1}}{rX} \left(\frac{-2I^8 + 10I^6 - 12I^4 \ln I - 9I^4 + 2I^2 - 1}{12I^2 \left(I^4 - 4I^2 + 4 \ln I + 3 \right)} \right), \end{split}$$

which for a large diffuser $I \approx 1$ simplifies to

$$M_{\text{mix}} \approx \frac{3}{8} \Gamma \hat{p}_0 \omega^{-1} \mathcal{L} \widehat{rX}^{-1} (1 - I). \tag{54}$$

Reintroducing the scalings gives the final result that the total liquid phase in the unaerated region is approximately given by:

$$M_{\text{mix}} = \frac{3 g \rho_l U_l (1 - I)}{8 r X R T}.$$
 (55)

The key finding here is that as the bubble radius decreases, the mixing is independent of the bubble radius and the column height. This assertion is based on derivation for the amount of dissolved gas in the unaerated region (M_mix). The exact solution, (based on velocity field) is the integral (52). We use a series of asymptotic techniques to reduces the integral (52) to Eq. (55), where the bubble radius does not appear in the equation. To verify/valid our calculation, we perform the integral (52) exactly, (see Fig. 7), and we find that for large omega (small bubble radius), the results agree with the analysis, and M_{mix} no longer increases. Although it should be noted that for close to unity aspect

ratios, Al-Mashhadani et al. (2015) found that liquid mixing rates could still increased by a factor of ten with a reduction from 1 mm to 0.1 mm diameter bubbles. Also of note is the effect of biomass growth, which will explicitly affect the equation by increasing rX. Increasing biomass will reduce the mixing which we attribute to more of the dissolved gas being stripped by the biomass, which produces great inhomogeneity.

4.6. Slow degassing

As $\omega \to 0$, to leading order Eq. (45) is given by

$$(\hat{\mathbf{u}} \cdot \nabla) Y = \mathcal{L}F(r) - r\widehat{X}Y. \tag{56}$$

Applying the transformation $s=r, \tau=\hat{p}_0^{-1}(1-z)^{-1}rU(r)$, the equation reduces to

$$-\frac{p_0\tau^2}{sU(s)}\frac{\partial Y}{\partial s} = s\left(\mathscr{L}F(s) - r\widehat{X}Y\right).$$

We will perform the same calculation as in the quick degassing case, where we divide the solution into two domains $s \leq I$, and s > I. In the aerated region we assume that the liquid phase fraction is in equilibrium, i.e, $Y = \frac{\mathscr{L}}{rX}$. In the unaerated region, there is no source term, hence the general solution is

$$Y = B(\tau) \exp\left(\widehat{rX} p_0^{-1} \tau^{-2} \int_1^r s^2 U(s) \, \mathrm{d}s\right). \tag{57}$$

Unlike for the large ω case, the streamlines propagate from the unaerated region to the aerated region in our model. To conserve mass there must be a small region at the top, of the order $\mathcal{O}(\varepsilon)$, where the stream-lines go from the aerated region to the unaerated region. In this region the liquid phase fraction quickly propagates. We assume that this happens sufficiently quickly that there is little change in Y_I . To model this we have the boundary condition at $\hat{z} = \frac{H}{L\hat{p}_0}$, $Y = \frac{\mathcal{L}}{rX}$. B can determined numerically by inverting r as a function of T on the boundary which we will do in the following section. We can make analytical progress by again deploying the large diffuser approximation ($I \approx 1$) where $U(r) \approx \frac{1}{4a^2}I(1-I^2)(r-1)^2$, which results in the analytical solution

$$Y = \frac{\mathcal{L}}{r\widehat{X}} \exp\left(\chi(z) (1 - r)^{-1}\right), \quad \chi(z) = \beta (1 - z)^2 \left(\frac{\left(1 - \frac{H}{L\hat{\rho}_0}\right)^{\frac{3}{2}}}{(1 - z)^{\frac{3}{2}}} - 1\right), \quad (58)$$

where

$$\beta = \frac{4\alpha^2 r \widehat{X} \hat{p_0}^{-3}}{3I(1 - I^2)}.$$

5. Application to Fusarium venenatum

5.1. Parametric study

We now apply the theory to the large vessel (10 m height with an aspect ratio $\varepsilon=\frac{1}{10}$) containing *Fusarium venenatum* with the diffuser occupying 80% of the base (I=0.8). We will consider bubbles with radii in the range 1 cm to 1 mm. The temperature dependence of Henry's constant for oxygen is given by $H_e\approx0.03$ for 28 °C< T<30 °C (Sander, 2015) (which is the temperature range reported by Wiebe (2002)). The flow-rate is chosen so that the gas hold up is 10% above the diffuser, which can be achieved by Eq. (9) for 1 mm bubbles which results in $Q=0.01~{\rm m}^3~{\rm s}^{-1}$. We assume a viscosity of 0.1 Pa, in line with our previous simulations.

The remaining parameter to deduce is the oxygen uptake rate (OUR), although to the author's knowledge there are no reported values for the OUR of *Fusrium veneatum* in the literature. To achieve a coarse approximation, we will assume that the oxygen uptake rate is a representative value to that of a hyphae of Neurospora crassa. Lew and Levina (2004) give the oxygen influx on the order of 10 nmole cm 2 s $^{-1}$.

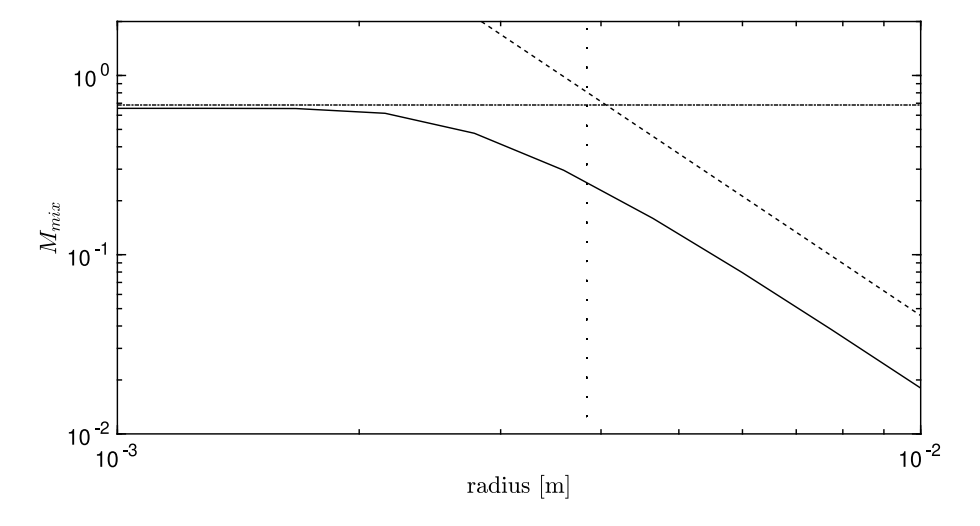


Fig. 7. M_{mix} (dimensionless) as a function of bubble radius. The exact integral (52) for the large ω solution is denoted by the solid line and the approximation (55) by the dot dashed line. The full integral solution for the small ω case is denoted by the dashed line. The bubble radius for which $\omega = 1$ is indicated by the dotted line.

Table 1
Parameter values.

Parameter	Value
Н	10 m
L	1 m
r_d	80 cm
H_e	0.03
Q	$0.01 \text{m}^3 \text{s}^{-1}$
μ	0.1 Pa s
OUR	$5 \times 10^{-3} \text{ kg m}^{-3} \text{ s}^{-1}$
rX	$1.4 \times 10^{-3} \text{ kg m}^{-3} \text{ s}^{-1}$

By analysing the two dimensional image of *Fusarium venenatum* from Wiebe (2002) and assuming cylindrical symmetry, we can calculate the surface to volume ratio to be 1 nm $^{-1}$. The volume fraction of *Fusarium venenatum* is assumed to be 0.1. This volume phase fraction was selected as a representative value, and it chosen as the order of magnitude to the maximum random packing value for ellipsoids is approximately 0.7 (Chaikin et al., 2006), Zhou et al. (2011). We can use these three values to calculate the OUR to be 5×10^{-3} kg m $^{-3}$ s $^{-1}$. As this calculation is for a constant uptake-rate, but we are analysing the oxygen limited case, whereby OUR will be given by

$$rXY_{l}, (59)$$

the OUR is also a function of liquid phase fraction Y_l in addition to rX. As we wish to the oxygen uptake to be 5×10^{-3} kg m⁻³ s⁻¹, we choose rX such that this is the maximum possible uptake rate OUR to occur for our selected range of bubble radii. This leads to the scaled rX value 1.4×10^{-3} kg m⁻² s⁻¹.

For the ease of the reader the parameters obtained are summarized in Table 1. Due to the quantity of assumptions required in forming the rX value and the errors incurred therein, we will explore the effect of varying rX on the mixing in the following section.

5.2. Effect of bubble radius

The effect of changing the bubble radius on the variables $M_{\rm mix}$ and $M_{\rm eff}$ is shown in Figs. 7 and 8, respectively. We seek approximate dynamics for the large ω case, mixing slowly increases as the bubble radius is reduced. The asymptotic solution (55) predicts no change for bubble radii less than 2 mm ($\omega \approx 7$). For the small ω limit we see

the dissolved gas increases with a power-law relationship. This can be deduced as β in the large diffuser limit equation is extremely small, hence $Y \approx \Gamma \frac{\mathcal{L}}{PX}$ which increases like a^{-3} . For $r \approx 4$ mm, ω is $\mathcal{O}(1)$ and will start to plateau to the large ω solution. Overall we find that decreasing the bubble size from 1 cm to 1 mm should result in an order of magnitude increase in the dissolved gas in the unaerated region.

The dependence of total oxygen flux $M_{\rm eff}$ on bubble radius is shown in Fig. 8. We can clearly see an increase in flux as the radius decreases and the change in behaviour from a^{-5} to a^{-2} for bubbles around 4 mm.

Due to the coarse approximation in obtain a value for the OUR, we sweep the parameter over a several orders of magnitude to account for the degree of uncertainty into this value. The effect of the OUR on M_{mix} is shown in Figs. 9(a) and 9(b). From Fig. 9(a) we can observe that our large ω approximation is valid for the chosen rX values and from Fig. 9(b) that as rX decreases the mixing is increases like rX^{-1} . As our mixing metric is the quantity of dissolved gas in the unaerated region, we attribute this to the dissolved gas being consumed a greater rate, which effectively causes an oxygen poor region, and thus insufficient mixing. In Fig. 9(b), there is a disparity between Laplace's approximation and the integral (52) is due to $\omega \approx 2$ for our selected values, which causes an error in the large ω approximation.

6. Conclusions

The principal result of the paper is a detailed analysis of the predicted flow field induced by a cloud of bubbles flowing with and without mass transfer. We find that for oxygen starved mycelia (or other cultured microorganism) the total oxygen transfer to the bubble increases like a^{-2} for smaller bubbles and a^{-5} for larger ones. The other key finding is the total oxygen concentration in the unaerated region cannot be increased by reducing the bubble radius below 2 mm for our selected parameters. However, an order of magnitude increase is possible by reducing the radius of bubbles from cm to mm. However, there are several assumptions which limit the result. In numerical validation of the hydrostatic pressure driven flow, as the bubble radius is decreased, the model significantly overpredicts the fluid velocity. The model also necessitates that the aspect ratio be smaller than the Reynolds number i.e. αRe be small. For a low viscosity medium this condition is difficult to achieve. It should be noted that a small increase in biomass can result in a large increase in viscosity (Riley et al., 2000). However, for low concentrations of biomass (Deindoerfer and West, 1960) or pelleted mycelia (Kim et al., 1983; Metz and Kossen, 1977),

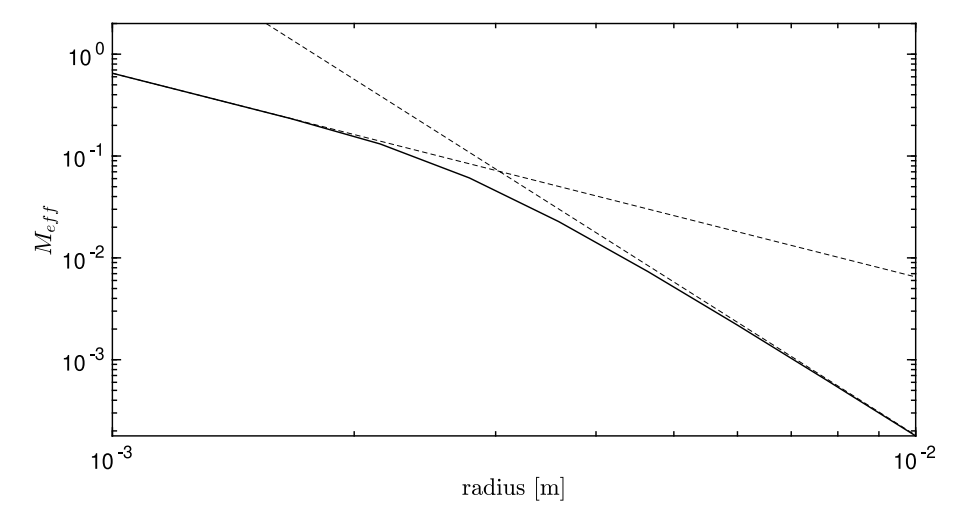
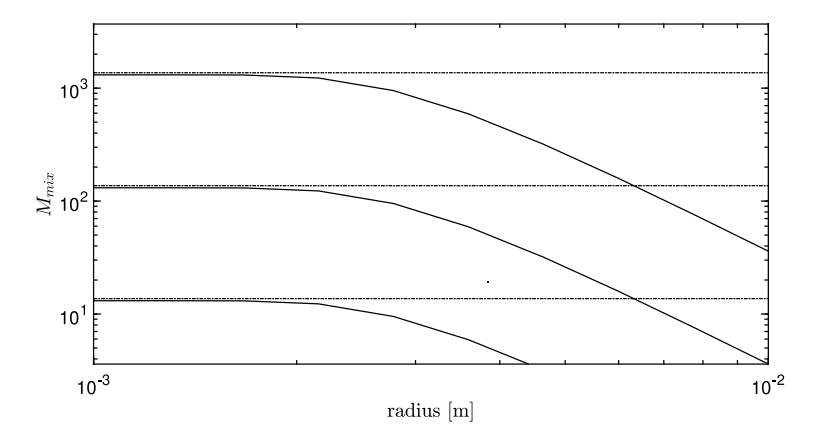
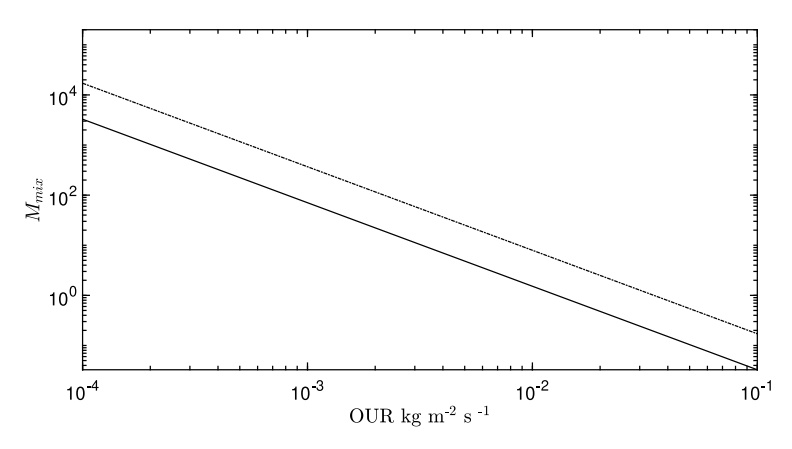


Fig. 8. $M_{\rm eff}$ as a function of bubble radius (solid line). The small bubble (a^{-2}) and large bubble (a^{-5}) behaviours are indicated by the dashed line.



(a) A plot of M_{mix} again the radius [m] for different rX values. The two curves are the exact integral (52), and the dashed is the approximation (55). The upper, middle and lower sets of curves are for OUR $\times 10^{-5}$, 5×10^{-4} , 5×10^{-3} kg m ⁻²s ⁻¹. The normalising rX chosen for the 5×10^{-3} kg m ⁻²s ⁻¹.



(b) A plot of the mixing metric M_{mix} against the OUR. The other parameters have the values as outlined in section 5.1.

Fig. 9. The effect of (a) rX and (b) OUR on the mixing metric.

the system will remain mostly Newtonian fluid, where our model would still be applicable. Once the biomass increases, many mycelial suspensions can result in viscoplastic or shear-thinning/thickening behaviour (Doran, 2013; Bliatsiou et al., 2020; Pollard et al., 2002), which would

affect the regime of applicability of our model, necessitating deeper rheological treatment for the model to be valid. Nonetheless, pelleted mycelia often behave more like a Newtonian fluid. These areas require further study to properly quantify the mixing effects.

CRediT authorship contribution statement

S. Chaffin: Conceptualization, Formal analysis, Methodology, Writing – original draft. N.A.M. Monk: Conceptualization, Formal analysis, Methodology, Writing – review & editing. J.M. Rees: Conceptualization, Formal analysis, Methodology, Writing – review & editing. W.B. Zimmerman: Conceptualization, Formal analysis, Funding acquisition, Methodology, Resources, Writing – original draft, Writing – review & editing.

Declaration of competing interest

The authors declare that they have no known competing financial interests or personal relationships that could have appeared to influence the work reported in this paper.

Acknowledgements

The authors gratefully acknowledge the Engineering and Physical Sciences Research Council (EPSRC), UK for supporting this work financially (Grant No. EP/N011511/1), simultaneously with InnovateUK (IB Catalyst Programme), UK. The authors would like to thank Pratik Desai and Michael Hines of Perlemax Ltd. for helpful discussions.

References

- Abdulrazzaq, N.N., Al-Sabbagh, B.H., Rees, J.M., Zimmerman, W.B., 2016. Purification of bioethanol using microbubbles generated by fluidic oscillation: A dynamical evaporation model. Ind. Eng. Chem. Res. 55 (50), 12909–12918.
- Al-Mashhadani, M.K.H., Wilkinson, S.J., Zimmerman, W.B., 2015. Airlift bioreactor for biological applications with microbubble mediated transport processes. Chem. Eng. Sci. 137, 243–253.
- Anderson, C., LeGrys, G.A., Solomons, G.L., 1982. Concepts in the design of large-scale fermenters for viscous culture broths. Chem. Eng. 377, 43–49.
- Becze, G.D., Liebmann, A.J., 1944. Aeration in the production of compressed yeast. Ind. Eng. Chem. 36 (10), 882–890.
- Bliatsiou, C., Schrinner, K., Waldherr, P., Tesche, S., Böhm, L., Kraume, M., Krull, R., 2020. Rheological characteristics of filamentous cultivation broths and suitable model fluids. Biochem. Eng. J. 163, 107746.
- Calahorra, M., Sánchez, N.S., Peña, A., 2009. Activation of fermentation by salts in Debaryomyces Hansenii. FEMS Yeast Res. 9 (8), 1293–1301.
- Chaikin, P.M., Donev, A., Man, W., Stillinger, F.H., Torquato, S., 2006. Some observations on the random packing of hard ellipsoids. Ind. Eng. Chem. Res. 45 (21), 6960–6965.
- Chambergo, F.S., Valencia, E.Y., 2016. Fungal biodiversity to biotechnology. Appl. Microbiol. Biotechnol. 100 (6), 2567–2577.
- Chisti, Y., Moo-Young, M., 1986. Disruption of microbial cells for intracellular products. Enzyme Microb. Technol. 8 (4), 194–204.
- Crabtree, J., Bridgwater, J., 1969. Chain bubbling in viscous liquids. Chem. Eng. Sci. 24, 1755–1768.
- de Jesus, S.S., Neto, J.M., Filho, R.M., 2017. Hydrodynamics and mass transfer in bubble column, conventional airlift, stirred airlift and stirred tank bioreactors, using viscous fluid: A comparative study. Biochem. Eng. J. 118, 70–81.
- Deindoerfer, F.H., West, J.M., 1960. Rheological properties of fermentation broths. Adv. Appl. Microbiol. 2, 265–273.
- Desai, P.D., Hines, M.J., Riaz, Y., Zimmerman, W.B.J., 2018. Resonant pulsing frequency effect for much smaller bubble formation with fluidic oscillation. Energies 11 (10).
- Desai, P., Zimmerman, W., 2023a. Microbubble intensification of bioprocessing: The role of direct microorganism and bubble interactions. 2023. Johnson Matthey Technol. Rev. 67 (4), 371–401. http://dx.doi.org/10.1595/205651323x16778518231554.
- Desai, P., Zimmerman, W., 2023b. Transient effects and the role of wetting in microbubble generation. Curr. Opin. Colloid Interface Sci.
- Doran, P.M., 2013. Bioprocess Engineering Principles, Second Edition, second ed. Academic Press Waltham, Mass, Waltham, Mass..
- Finnigan, T., Needham, L., Abbott, C., 2017. Mycoprotein: A healthy new protein with a low environmental impact. In: Sustainable Protein Source. Academic Press, San Diego, pp. 305–325.
- Finnigan, T., Wall, B., Wilde, P., Stephens, F., Taylor, S., Freedman, M., 2019. Mycoprotein: The future of nutritious nonmeat protein, a symposium review. Curr. Develop. Nutrition 3, nzz021.
- Garcia-Ochoa, F., Gomez, E., Alcon, A., Santos, V.E., 2013. The effect of hydrodynamic stress on the growth of *Xanthomonas* campestris cultures in a stirred and sparged tank bioreactor. Bioprocess Biosyst. Eng. 36 (7), 911–925.

- Gaskell, P., Savage, M., Summers, J., Thompson, H., 1998. Stokes flow in closed, rectangular domains. Appl. Math. Model. 22 (9), 727–743.
- Gélinas, P., 2016. Aeration and foam control in Baker's Yeast Production: Mapping patents. Comprehens. Rev. Food Sci. Food Saf. 15 (2), 371–391.
- Gilmour, D.J., Zimmerman, W.B.J., 2020. Microbubble intensification of bioprocessing. Adv. Microb. Physiol. 77, 1–35.
- Hanotu, J., Kong, D., Zimmerman, W.B.J., 2016. Intensification of yeast production with microbubbles. Food Bioprod. Process. 100, 424–431.
- Hosseini, S.M., Khosravi-Darani, K., Mohammadifar, M.A., Nikoopour, H., 2009. Production of mycoprotein by *Fusarium* venenatum growth on modified vogel medium. Asian J. Chem. 21, 4017–4022.
- Jackson, A.T., 1985. Some problems of industrial scale-up. J. Biol. Educ. 19 (1), 48–52.Joseph, D.D., 1977. The convergence of biorthogonal series for biharmonic and Stokes flow edge problems. Part I. SIAM J. Appl. Math. 33 (2), 337–347.
- Kaster, J.A., Michelsen, D.L., Velander, W.H., 1990. Increased oxygen transfer in a yeast fermentation using a microbubble dispersion. Appl. Biochem. Biotechnol. - A 24–25 (1), 469–484.
- Kazakis, N.A., Mouza, A.A., Paras, S.V., 2008. Experimental study of bubble formation at metal porous spargers: Effect of liquid properties and sparger characteristics on the initial bubble size distribution. Chem. Eng. J. 137 (2), 265–281.
- Kim, J.H., Lebeault, J.M., Reuss, M., 1983. Comparative study on rheological properties of mycelial broth in filamentous and pelleted forms. Eur. J. Appl. Microbiol. Biotechnol. 18 (1), 11–16.
- Kulkarni, A.V., Joshi, J.B., 2011. Design and selection of sparger for bubble column reactor. Part I: Performance of different spargers. Chem. Eng. Res. Des. 89 (11), 1972–1985.
- Lebrun, G., Xu, F., Le Men, C., Hébrard, G., Dietrich, N., 2021. Gas-liquid mass transfer around a rising bubble: Combined effect of rheology and surfactant. Fluids 6 (2).
- Lonchamp, J., Clegg, P.S., Euston, S.R., 2019. Foaming, emulsifying and rheological properties of extracts from a co-product of the Quorn fermentation process. Eur. Food Res. Technol. 245 (9), 1825–1839.
- Metz, B., Kossen, N.W.F., 1977. The growth of molds in the form of pellets-A literature review. Biotechnol. Bioeng. 19 (6), 781–799.
- Mikko, M., Taivassalo, V., Kallio, S., 1996. On the Mixture Model for Multiphase Flow, vol. 288, VTT Publications.
- Nienow, A.W., 2006. Reactor engineering in large scale animal cell culture. Enzyme Microb. Technol. (50), 9–33.
- Pandurangan, P., Raja, N., Sunkar, S., 2015. Design of medium components for the enhanced production of mycoprotein by *Fusarium* venenatum using plackett burman model. Res. J. Pharmaceut. Biol. Chem. Sci. 6, 1251–1255.
- Panton, R.L., 1984. Incompressible Flow. John Wiley & Sons, New York.
- Pollard, D., Hunt, G., Kirschner, T., Salmon, P., 2002. Rheological characterization of a fungal fermentation for the production of pneumocandins. Bioprocess Biosyst. Eng. 24 (6), 373–383.
- Porcel, E., Lopez, J., Perez, J., Sevilla, J., Chisti, Y., 2005. Effects of pellet morphology on broth rheology in fermentations of aspergillus terreus. Biochem. Eng. J. 26 (2–3), 139–144.
- Rahman, S., Andersson, B., Irandoust, S., Bouaifi, M., 2002. Bubble Size and Coalescence Rate in a Gas-Liquid Stirred Tank Reactor: Experimental and Theoretical Investigations.
- Rees-Zimmerman, C.R., Chaffin, S.T., 2021. Modelling the effect of bioreactor height on stripping fermentation products from the engineered bacterium *Geobacillus* thermoglucosidasius. Biochem. Eng. J. 176, 108195.
- Rehman, F., Medley, G.J., Bandulasena, H., Zimmerman, W.B., 2015. Fluidic oscillator-mediated microbubble generation to provide cost effective mass transfer and mixing efficiency to the wastewater treatment plants. Environ. Res. 137, 32–39.
- Reihani, S.S.F., Khosravi-Darani, K., 2019. Mycoprotein production from date waste using *Fusarium* venenatum in a submerged culture. Appl. Food Biotechnol. 5 (4), 243–352.
- Ribeiro, C., Lage, L., 2004. Experimental study on bubble size distributions in a direct-contact evaporator. Braz. J. Chem. Eng. 21 (1), 69–81.
- Ribeiro, C., Lage, L., 2005. Gas-liquid direct-contact evaporation: A review. Chem. Eng. Technol. 28 (10), 1081–1107.
- Riley, G.L., Tucker, K.G., Paul, G.C., Thomas, C.R., 2000. Effect of biomass concentration and mycelial morphology on fermentation broth rheology. Biotechnol. Bioeng. 68 (2), 160–172.
- Rzehak, R., Krepper, E., 2016. Euler-Euler simulation of mass-transfer in bubbly flows. Chem. Eng. Sci. 155, 459–468.
- Sander, R., 2015. Compilation of Henry's law constants for water as solvent. Atmos. Chem. Phys. 15 (8), 4399–4981.
- Sokolichin, A., Eigenberger, G., Lapin, A., 2004. Simulation of buoyancy driven bubbly flow: Established simplifications and open questions. AIChE J. 50 (1), 24–45.
- Sossa-Echeverria, J., Taghipour, F., 2015. Computational simulation of mixing flow of shear thinning non-Newtonian fluids with various impellers in a stirred tank. Chem. Eng. Process. 93, 66–78.
- Svensson, S.E., Bucuricova, L., Ferreira, J.A., Souza Filho, P.F., Taherzadeh, M.J., Zamani, A., 2021. Valorization of bread waste to a fiber and protein rich fungal biomass. Fermentation 7 (2).
- Swiderski, K., Narayanan, C., Lakehal, D., 2016. Application of *N*-phase algebraic slip model and direct quadrature method of moments to the simulation of air-water flow in vertical risers and bubble column reactor. Comput. Chem. Eng. 90, 151–160.

Wiebe, M., 2002. Myco-protein from *Fusarium* venenatum: A well established product for human consumption. Appl. Microbiol. Biotechnol. 58 (4), 421–427.
Zhou, Z.-Y., Zou, R.-P., Pinson, D., Yu, A.-B., 2011. Dynamic simulation of the packing of ellipsoidal particles. Ind. Eng. Chem. Res. 50 (16), 9787–9798.

Zimmerman, W., Tesař, V., Bandulasena, H., 2011. Towards energy efficient nanobubble generation with fluidic oscillation. Curr. Opin. Colloid Interface Sci. 16 (4), 350–356.

Zimmerman, W.B., Tesař, V., Butler, S., Bandulasena, H.C.H., 2008. Microbubble generation. Recent Patents Eng. 2 (1), 1–8.